Resonant micro-Raman spectroscopy of aligned single-walled carbon nanotubes on *a*-plane sapphire

Lewis Gomez-De Arco, Bo Lei, Stephen Cronin, and Chongwu Zhou[a)]
Department of Electrical Engineering, University of Southern California, Los Angeles, California 90089, USA

(Received 21 April 2008; accepted 17 August 2008; published online 24 September 2008)

Resonant micro-Raman spectroscopy was employed to characterize aligned single-walled carbon nanotubes grown on *a*-plane sapphire to address the alignment mechanism, the metal-to-semiconductor ratio, and the substrate surface influence in nanotube alignment and straightness. Nanotubes aligned predominantly following the $[1\bar{1}00]$ direction on the *a*-plane instead of the atomic step direction. Detailed analysis of radial breathing mode (RBM) and *G* bands revealed a metallic to semiconducting nanotube ratio of 1:2.6. Improved straightness of nanotubes grown on annealed substrates was attributed to stronger nanotube-substrate interaction along specific lattice directions during growth and confirmed by *G'* band broadening and damping of the RBM band. © *2008 American Institute of Physics*. [DOI: 10.1063/1.2979701]

Nanotube misalignment represents a serious drawback toward large scale fabrication of nanotube-based high performance devices.[1,2] Different methods have been developed to produce aligned single-walled carbon nanotube (SWCNT) arrays, among which the epitaxial approach has emerged as a scalable process to produce massively aligned nanotubes on insulating substrates such as sapphire and quartz.[2–7] Epitaxial growth alignment can be understood by considering the presence of strong binding energies localized along low potential energy directions, defect sites, and atomic steps on the substrate surface.[8] There is, however, controversy, as aligned growth has ben explained as guided by the substrate atomic steps and surface potential, for quartz and sapphire, respectively.[5,6] In addition, there has been a lack of information about the metal-to-semiconductor ratio and the effect of the nanotube-substrate interaction on Raman bands for such aligned nanotubes.

In this paper, we combined microfabrication techniques and multiwavelength resonance micro-Raman spectroscopy to shed light on the alignment mechanism, metal-to-semiconductor ratio, and substrate surface influence in the alignment and straightness of as-grown nanotubes on *a*-plane sapphire.

Aligned SWCNTs used in this study were synthesized on *a*-plane sapphire by chemical vapour deposition (CVD). Ferritin protein (Alpha Aesar, Inc.) was used as the iron source for catalyst particles. The growth of aligned nanotubes was fulfilled by flowing 2000 SCCM (SCCM denotes cubic centimeter per minute at STP) of CH_4, 10 SCCM of C_2H_4, and 600 SCCM of H_2 at 900 °C. Simultaneous control of nanotube orientation and position was achieved by patterning catalyst at desired sites on the sapphire substrates. After synthesis, atomic force microscopy (AFM) and field-emission scanning electron microscopy (FESEM) combined with micro-Raman spectroscopy were used to provide information of the samples at individual nanotube level.

Figure 1(a) shows an AFM image of a clean *a*-plane sapphire substrate where atomic steps can be observed along the $[\bar{1}101]$ lattice direction. AFM image in Fig. 1(b) shows that as-grown nanotubes did not align along the substrate atomic steps direction but rather followed the $[1\bar{1}00]$ direction on the *a*-face. In addition, Fig. 1(b) shows that a few nanotubes had short sections exhibiting alignment along the atomic step direction $[\bar{1}101]$, suggesting the presence of competitive alignment mechanisms of nanotubes on *a*-sapphire. Competition between lattice-directed and atomic-step-templated alignment mechanisms has been reported for nanotubes grown on substrates with different miscut angles.[9] However, in our case the substrates lacked of intentional miscut and a lattice oriented alignment mechanism was strikingly favored over the atomic step one. Furthermore, Fig. 1(c) depicts the top and side views of the *a*-sapphire atomic layout as well as a schematic showing the nanotube principal alignment direction. Low van der Waals energy grooves of about 4.34 Å wide and 0.91 Å deep present between oxygen atoms on the upmost layer of the sapphire substrate along the $[1\bar{1}00]$ direction, provide a high binding energy path that added to the lack of miscut on the substrate, could

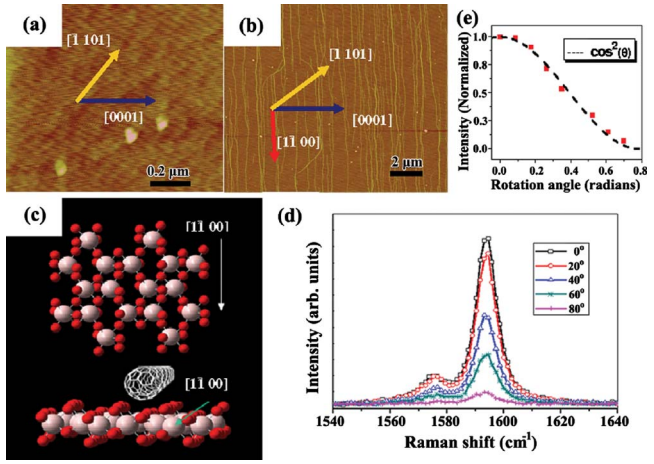

FIG. 1. (Color online) (a) AFM image of *a*-sapphire substrate showing the *c*-axis and the atomic step direction. (b) AFM image of CVD-grown SWCNTs on *a*-sapphire. (c) Top (upper) and side (lower) views of the *a*-sapphire surface atomic structure. (d) *G* band Raman intensity dependence on the polarization angle. (e) $\cos^2(\theta)$ fit to the plot of the normalized *G* band intensity vs the polarization angle (scattered dots).

a)Electronic mail: chongwuz@usc.edu.

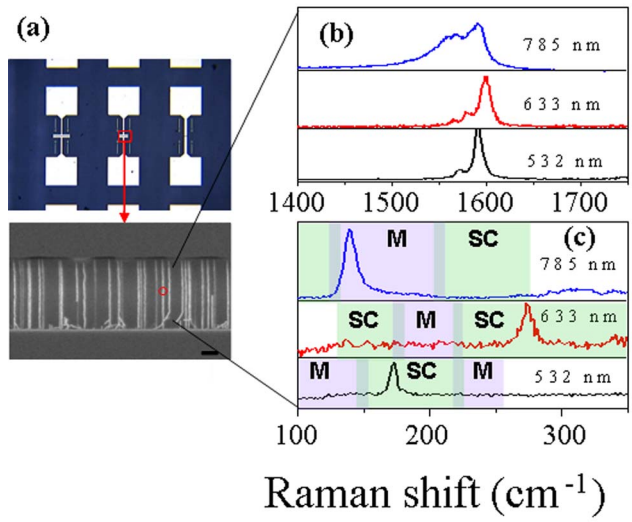

FIG. 2. (Color online) (a) Optical and SEM images of a device, showing aligned nanotubes between patterned source and drain electrodes. Scale bar is 2 μm. (b) RBM and (c) *G* band of several typical nanotubes scanned with lasers of 785, 633, and 532 nm in wavelength from top to bottom, respectively.

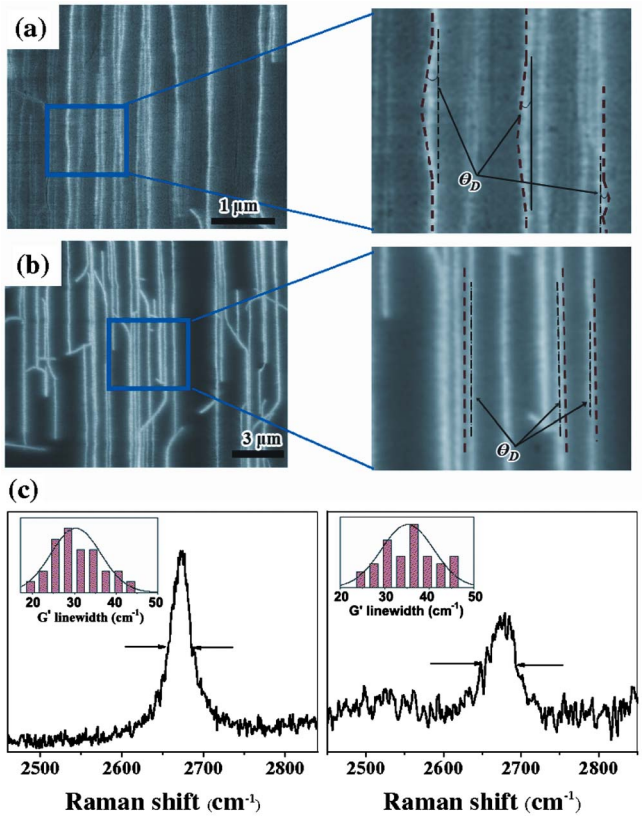

FIG. 3. (Color online) FESEM images of aligned nanotubes synthesized on (a) unannealed and (b) annealed *a*-sapphire. Deviation angles from the direction $[1\bar{1}00]$ (θ_D) in nanotube segments aligned in that direction were typically ten times lower in nanotubes grown on annealed sapphire, evidencing higher straightness than nanotubes grown on unannealed sapphire. (c) Representative G' band spectra for SWCNTs grown on unannealed (upper) and annealed (lower) *a*-sapphire. Insets in (d): G' FWHM distribution measured by Lorentzian fitting of Raman peaks.

explain the favored lattice-directed alignment.

Figure 1(d) shows plots of *G* band intensity as a function of the angle of polarization (θ). It is observed that the Raman signal is strongly suppressed when the excitation laser is polarized perpendicular to the nanotube axis, following the antenna effect. As the probability of the absorption and emission processes varies linearly with the intensity of the incident field, which in turn varies as $\cos^2(\theta)$, it is expected that the Raman *G* band signal shows a close fit to this polarization dependence.[5,10] This dependence is clearly shown in Fig. 1(e) and remained throughout the samples. The results obtained reveal a high degree of unidirectional alignment from the collectivity of nanotubes along the $[1\bar{1}00]$ of the *a*-plane, therefore confirming lattice-guided alignment as the predominant alignment mechanism on *a*-plane sapphire without intentional miscut.

The distribution of the electronic nature of isolated carbon nanotubes was investigated by analyzing the tangential vibration modes (G_- and G_+ bands) and the radial breathing mode (RBM) frequencies of carbon nanotubes grown from patterned catalyst particles between metallic electrodes. Figure 2(a) shows optical and SEM images of nanotubes aligned between source and drain electrodes. Raman spectra were acquired on the device channels with a spatial resolution of $\sim$0.5 μm. G_- band for semiconducting nanotubes exhibited a typical Lorentzian line shape, while metallic nanotubes showed a broadened Breit–Wigner–Fano G_- line shape due to the presence of free electrons in the conduction band.[11,12] FESEM images and micro-Raman provided enough resolution to correlate individual nanotubes with their Raman spectra and determine the number of nanotubes exhibiting semiconducting or metallic characteristics in the samples. Figures 2(b) and 2(c) show typical micro-Raman spectra in the RBM and *G* band frequency regions, respectively, for individual aligned nanotubes. We correlated nanotube diameters with their RBM frequency by $d_t = A/(\omega_{\mathrm{RBM}} - B)$, where d_t is the nanotube diameter, ω_{RBM} is the RBM frequency, $A = 248$, and $B = 0$.[11] A typical assignment is described for the spectra at the bottom of Figs. 2(b) and 2(c). For this nanotube, the *G* band line shape reveals a semiconducting nature and its RBM frequency (174.65 cm^{-1}) obtained with a 2.33 eV (532 nm) laser corresponds to a resonant semiconducting nanotube with $d_t = 1.42$ nm. This assignment was confirmed by calculating the bandgap energies of a nanotube with this diameter. Tight binding calculations and tunable Raman spectroscopy show that only semiconducting nanotubes for which $E_{33} \sim 2.30$ eV will be resonantly excited by this laser.[12] Applying this procedure to more than 150 nanotubes and using lasers with energies 1.58 eV (785 nm), 1.98 eV (633 nm), and 2.33 eV (532 nm) we determined the averaged percentage of metallic nanotubes, for two different CVD-grown samples, to be about $(27.9 \pm 0.6)\%$; corresponding to a ratio between aligned metallic and semiconducting nanotubes of 1:2.6, which is moderately lower than the theoretically predicted 1:2 ratio.[13]

Raman G' band intensity and line shape of carbon nanotubes can be related to strain and external perturbation.[14] In order to probe the effect of nanotube-substrate interactions on Raman G' band, aligned nanotubes were grown on unannealed [Fig. 3(a)] and annealed [Fig. 3(b)] *a*-sapphire substrates. The annealing condition was 900°C in air for 13 hours. Comparison of Figs. 3(a) and 3(b) reveals a higher degree of straightness on nanotubes grown on annealed *a*-sapphire, but at the same time, alignment of small fractions of nanotubes in directions other than $[1\bar{1}00]$ becomes evident. That is because the annealing process can induce re-

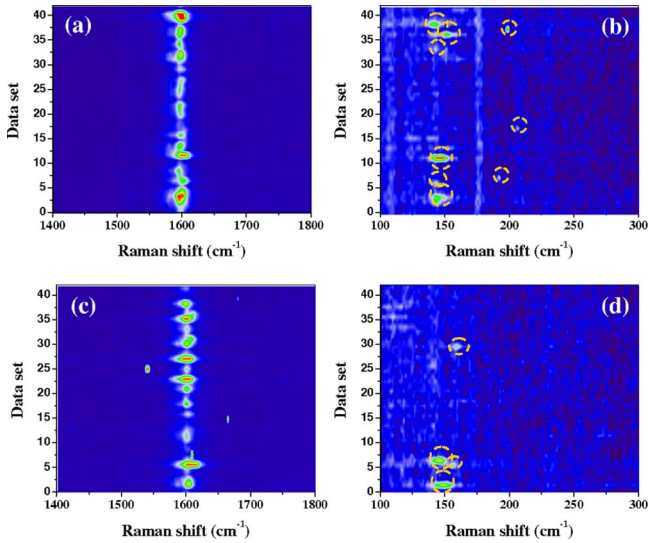

FIG. 4. (Color online) Intensity profile of the (a) resonant Raman RBM and (b) *G* band with respect to the scan position of aligned nanotubes grown on unannealed *a*-plane sapphire. RBM peaks have been circled for clarity. (c) and (d) show the Raman intensity profile of aligned nanotubes on annealed sapphire for RBM and *G*-band regions, respectively.

construction on *a*-sapphire surface,[15] leading to improved surface atomic ordering along $[1\bar{1}00]$ and thus straighter nanotubes. At the same time, annealing can also induce more pronounced step edges, therefore yielding nanotube segments along other directions. We note that even for annealed samples, the predominant alignment direction is still $[1\bar{1}00]$. On the other hand, the unannealed *a*-sapphire surface consists of irregular corrugations and scratches that allow nanotubes to hop between vicinal and disordered pseudounidimensional surface potential grooves. This may result in lowered straightness in the nanotubes, as shown in Fig. 3(a). To further confirm the importance of nanotube-substrate interactions in the straightness of aligned nanotubes, we analyzed the G' band linewidth distribution of nanotubes grown on unannealed and annealed *a*-sapphire. Upper and lower panels of Fig. 3(c) show representative G' band spectra of SWCNTs grown on unannealed and annealed *a*-sapphire, respectively. The average full width at half maximum (FWHM) of the G' band increased from 30.3 ± 5.0 to 35.1 ± 5.9 cm^{-1}, a total of around 4.8 cm^{-1} for nanotubes aligned on annealed *a*-sapphire. Line broadening of this band can occur as a result of a perturbation exerted on the nanotubes due to nanotube-substrate van der Waals interactions. Thus, an improved surface atomic ordering favors straightness on nanotubes due to a stronger substrate-SWCNT interaction, along the alignment direction.

The effect of the strength of nanotube-substrate interactions in Raman low frequency modes is shown in Fig. 4. We have consistently observed that the percentage of nanotubes showing distinguishable RBM bands is lower for nanotubes grown on annealed sapphire than for those grown on unannealed sapphire, and these surface effects were found to be more evident on small diameter nanotubes. RBM of nanotubes is a totally symmetric vibration A_1 in which all the carbon atoms undergo an equal radial displacement.[16] This mode is greatly affected under forces such as hydrostatic pressure and intermolecular Van der Waals interactions that can induce subtle geometrical deformations.[17–19] Results displayed in Fig. 4 suggest that annealed sapphire exerted stronger interaction with the aligned nanotubes than unannealed sapphire, therefore leading to a faster damping of the RBM vibration via mode symmetry breaking, which in turn yields lower intensity or disappearance of the RBM bands. This conclusion is consistent with the observation of G' band broadening for aligned nanotubes on annealed sapphire shown in Fig. 3(d). By RBM, being the only well resolved symmetric mode among the main carbon nanotube bands, it also explains why other modes remain visible.

In summary, we showed that micro-Raman spectroscopy can be used to probe nanotube-substrate interactions involved in the alignment mechanism of nanotubes on substrate surfaces. Furthermore, we found that at the synthesis conditions employed, the percentage of metallic nanotubes was not affected by nanotube-substrate interactions present in aligned growth. Results obtained in this work agree with the growth mechanistic concept of surface potential interactions in the self-alignment of nanotubes on *a*-plane sapphire.

We acknowledge support from the SRC FCRP FENA Center, and NSF CAREER Award.

[1] A. Ismach and E. Joselevich, Nano Lett. **6**, 1706 (2006).
[2] S. Han, X. Liu, and C. Zhou, J. Am. Chem. Soc. **127**, 5294 (2005).
[3] K. Ryu, A. Badmaev, L. Gomez, F. Ishikawa, B. Lei, and C. Zhou, J. Am. Chem. Soc. **129**, 10104 (2007).
[4] A. Ismach, D. Kantorovich, and E. Joselevich, J. Am. Chem. Soc. **127**, 11554 (2005).
[5] C. Kocabas, S. H. Hur, A. Gaur, A. Gaur, M. A. Meitl, M. Shim, and J. A. Rogers, Small **1**, 1110 (2005).
[6] H. Ago, N. Uehara, K. Ikeda, R. Ohdo, K. Nakamura, and M. Tsuji, Chem. Phys. Lett. **421**, 399 (2006).
[7] H. Ago, K. Nakamura, K. Ikeda, N. Uehara, N. Ishigami, and M. Tsuji, Chem. Phys. Lett. **408**, 433 (2005).
[8] G. A. Somorjai, Chem. Rev. (Washington, D.C.) **96**, 1223 (1996).
[9] H. Ago, K. Imamoto, N. Ishigami, R. Ohdo, K. Ikeda, and M. Tsuji, Appl. Phys. Lett. **90**, 123112 (2007).
[10] Y. Wang, K. Kempa, B. Kimball, J. B. Carlson, G. Benham, W. Z. Li, T. Kempa, J. Rybczynski, A. Herczynski, and Z. F. Ren, Appl. Phys. Lett. **85**, 2607 (2004).
[11] A. Jorio, M. A. Pimenta, A. G. Souza Filho, R. Saito, G. Dresselhaus, and M. S. Dresselhaus, New J. Phys. **5**, 139 (2003).
[12] M. S. Dresselhaus, G. Dresselhaus, A. Jorio, A. G. Souza Filho, and R. Saito, Carbon **40**, 2043 (2002).
[13] P. T. Araujo, S. K. Doorn, S. Kilina, S. Tretiak, E. Einarsson, S. Maruyama, H. Chacham, M. A. Pimenta, and A. Jorio, Phys. Rev. Lett. **98**, 067401 (2007).
[14] J. R. Wood, Q. Zhao, M. D. Frogley, E. R. Meurs, A. D. Prins, T. Peijs, D. J. Dunstan, and H. D. Wagner, Phys. Rev. B **62**, 7571 (2000).
[15] K. G. Saw, J. Mater. Sci. **39**, 2911 (2004).
[16] A. M. Rao, E. Richter, S. Bandow, B. Chase, P. C. Eklund, K. A. Williams, S. Fang, K. R. Subbaswamy, M. Menon, A. Thess, R. E. Smalley, G. Dresselhaus, and M. S. Dresselhaus, Science **275**, 187 (1997).
[17] U. D. Venkateswaran, A. M. Rao, E. Richter, M. Menon, A. Rinzler, R. E. Smalley, and P. C. Eklund, Phys. Rev. B **59**, 10928 (1999).
[18] M. J. Peters, L. E. McNeil, J. P. Lu, and D. Kahn, Phys. Rev. B **61**, 5939 (2000).
[19] X. Yang, G. Wu, J. Zhou, and J. Dong, Phys. Rev. B **73**, 235403 (2006).